IEEE Access
Multidisciplinary ⋮ Rapid Review ⋮ Open Access Journal

Received 8 December 2023, accepted 31 December 2023, date of publication 5 January 2024,
date of current version 11 January 2024.

Digital Object Identifier 10.1109/ACCESS.2024.3350555

RESEARCH ARTICLE

Partial Discharge Detection Based on Ultrasound Using Optimized Deep Learning Approach

ABDULAZIZ H. ALSHALAWI[1] AND FAHAD S. AL-ISMAIL[2,3,4], (Senior Member, IEEE)
[1]IPP Grid Integration and Studies, Saudi Power Procurement Company, Riyadh 13341, Saudi Arabia
[2]Department of Electrical Engineering, King Fahd University of Petroleum and Minerals (KFUPM), Dhahran 31261, Saudi Arabia
[3]Center for Environmental and Water, Research Institute, King Fahd University of Petroleum and Minerals (KFUPM), Dhahran 31261, Saudi Arabia
[4]K. A. CARE Energy Research and Innovation Center (ERIC), King Fahd University of Petroleum and Minerals (KFUPM), Dhahran 31261, Saudi Arabia

Corresponding author: Fahad S. Al-Ismail (fsalismail@kfupm.edu.sa)

This work was supported by the Deanship of Research Oversight and Coordination (DROC), King Fahd University of Petroleum and Minerals (KFUPM), under Project SL222001.

ABSTRACT Electrical equipment is prone to different types of Partial Discharge (PD) failures that are varying between minor and severe level. In this paper, Three developed models for Convolution Neural Network (CNN) are proposed to detect and classify four different partial discharge types which are arcing, corona discharge, tracking, looseness as well as healthy equipment situation. Notably, the resulting models exhibited an impressive overall accuracy of more than 94%, which is particularly significant considering the inherent presence of noise in the real-world samples obtained as representative field failures. These findings underscore the robustness and effectiveness of the CNN models in accurately identifying PDs, despite the intricate challenges associated with real-world data.

INDEX TERMS Acoustic emission, partial discharges, deep learning, optimization, Bayesian optimization, ultrasound detection, hyperparameter, short-time Fourier transform.

I. INTRODUCTION

Partial Discharge (PD) can be defined as the existence of a tiny vacancy in a solid insulator or a small gas bubble in a liquid insulator causes changes in the electric field distribution within the material. The dielectric constant of the void or gas bubble is lower than that of the surrounding insulating material, resulting in a higher electric field strength inside the void or gas bubble than the surrounding insulating material. In general, the occurrence of PD is a result of the local accumulation of electrical stress in specific areas of electrical insulation [1], [2].

PD can arise in a wide range of equipment that utilize different insulation materials and structures, including gas-insulated, oil-insulated, and solid-insulated devices. Any imperfection in the insulation may result in the emergence of PD. The nature of PD may differ depending on the equipment with distinct structures and insulation materials. PD can take place due to any of the following causes [3], [4]:

1) Rise of electric field intensity due to over stress.
2) Deterioration of the insulating material with age.
3) Local overheating which usually implant voids and bubbles.
4) Poor manufacturing which might introduce impurities in the insulation.
5) Bad installation or termination that accelerate insulation failure.

PD can take different forms and different names but as per IEC 60270 partial discharge is a general name for all forms which include Corona discharge, surface discharge and internal discharge [5]. Corona discharge can not be used interchangeably with the other two types as per IEC 60270 since corona usually take place in gaseous mediums only. Corona discharge is an electrical discharge that occurs due to the ionization of air in the vicinity of a high-voltage electrode. Surface discharge is a type of electrical discharge that takes place along the surface of a dielectric material, and it frequently occurs at the interface of two different materials [6]. Internal discharge usually takes place in weak insulation spots. This discharge is initiated by various factors such as the presence of cracks, contamination and air voids [7].

The associate editor coordinating the review of this manuscript and approving it for publication was Arpan Kumar Pradhan.

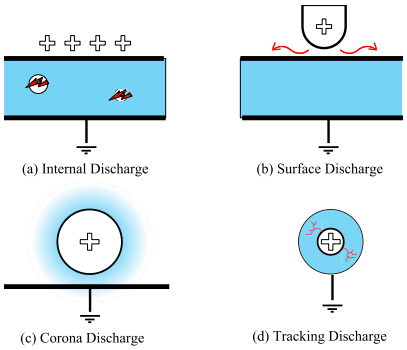

FIGURE 1. Types of partial discharge.

In Fig. 1, several forms of PD are illustrated. In Fig.1(a), internal discharge is shown where several voids are presented in the insulation medium which usually develop higher potential than the surrounding insulation medium. If PD is not repaired, then it will stress the insulation to develop a new form which is tracking (Fig.1(d)). Looseness (Fig.1(b)) is a sign of surface discharge that - if ignored - lead to flashover incident. Corona only takes place in gaseous mediums as it can be shown in the Fig.1(c) which is represented by the blue cloud around the conductor.

The methods employed for the detection of Partial Discharge can be classified into two categories: conventional and unconventional methods. The conventional method is a well-established electrical technique that adheres to the IEC-60270 standard for PD measurement. It involves measuring the apparent charge (q) across the terminal of the test object. However, it cannot be utilized on-site due to electromagnetic interference from the environment. In contrast, unconventional methods, including acoustic, Optical, Ultra High Frequency (UHF), and High Frequency Current Transformer (HFCT), detect high-frequency PD signals and are immune to electromagnetic interference as it can be seen in Fig. 2.

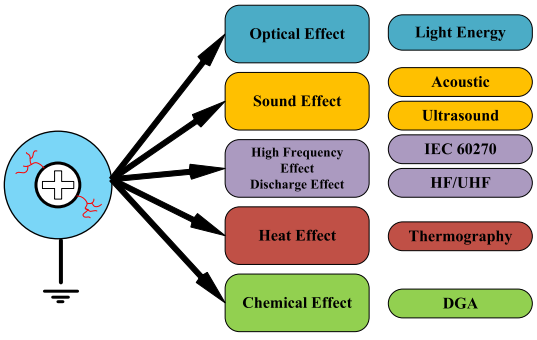

FIGURE 2. PD detection methods.

Electrical equipment is prone to different type of failures that vary between minor and severe levels, e.g. wiring looseness is usually considered as minor and usually is not expensive to be fixed. Other failures are considered severe and cost the organizations huge maintenance expenditure to repair or sometimes to replace the equipment such as Tracking.

This topic has caught many researches attention to study the phenomena and the effect on each equipment separately. For instance, in [8] the DC cables has been studied to investigate the effect of a DC electric field during transmission causing a buildup of electrical charges on the insulation surface. This led to an increase in local electric field strength which led to partial discharging. As the insulation's ability to withstand electricity decreases, it becomes easier for discharge channels to form, ultimately causing the insulating material to breakdown. A correlation model has been established to study the relationship between partial discharge ultrasonic waves and the amount of discharge in a DC cable. This model aims to analyze the mechanism of partial discharge and the ultrasonic properties of the cable.

High Voltage Direct Current (HVDC) cable system is also prone to frequent partial discharges. In [8], a correlation between PD ultrasound waves and number of discharges per cable is analyzed. Sagnac fiber detection system developed by utilizing the ultrasound characteristics of various insulation defects along with the repetition and magnitude of the PD. The impact of varying the length fiber sensing probes on the PD sensitivity has been studied using the frequency distribution characteristics of the PD. The accuracy tolerance of locating PD is within ± 80 m.

Harming discharges are not limited to DC cable, their effect can be extended to the insulators that carries the DC cables. Failure of the carrying insulators are a major source of power interruptions which impact the reliability of the grid. In order to maintain the reliability of the electric power system and meet the reliability standards, it is crucial to schedule inspection and ensure the proper functioning of insulators. The article in [9] presents the results of a laboratory study on distribution insulators failure prediction. The study involved applying 13.8 kV to a contaminated insulator and using an ultrasound detector connected to a computer to collect data. The data has been then analyzed using a hybrid deep learning technique called wavelet Long Short-Term Memory (LSTM) for time series prediction.

Transformers are major component of power systems since they link different voltage levels of the power grid and any malfunction in transformers can lead to significant costs in terms of downtime. Therefore, it is essential to detect in advance any potential issues to prevent unsafe conditions and minimize the expenses. Typically, faults in transformers developed due to either electrical or thermal stresses, may cause damages to the insulation oil in transformers. In oil-filled transformers, the insulation consists of cellulose and oil, and the decomposition of the insulation leads to the creation of gases that can dissolve in the oil. By performing dissolved gas analysis (DGA), it is possible to diagnose any faults in oil-filled transformers through analyzing the DGA composition percentages [10]. Traditional techniques for measuring PD in transformers, including the pulse current method, high-frequency current method, and dissolved gas

analysis method, are useful for identifying the onset of insulation degradation. However, these methods cannot accurately locate the PD sources within the transformer. These problems have been investigated in [11] and [12] utilizing intelligent techniques such as hybrid differential evolution (DE) algorithm and the particle swarm optimisation (PSO) algorithm and the results showed high accuracy of detection and localization.

Gas Insulated Switchgear (GIS) is another major part of electrical system which is also prone to PD issues. In [13], deep convolutional neural network (DCNN) has been developed to accurately recognize PD within GIS. The DCNN has shown high recognition precision when applied to PD pattern which is surpassing traditional machine learning algorithms. This method is particularly effective in handling data that involve high noise levels, which are commonly encountered in GIS studies. By training the DCNN on large dataset, it is possible to improve the accuracy of PD recognition even with the existence of high noise levels. Overall, the use of DCNN in PD recognition has shown promising results in improving the accuracy and reliability of PD detection in GIS applications.

Automated PD fault recognition of electrical equipment is a potential research area, specifically in the industry where equipment failure can have a significant impact on production capacity and employee safety. Neglecting active Partial Discharge in power cables, for instance, can lead to arc flash that may result in fatalities and fire. Identifying faults beforehand is necessary to prevent severe equipment damage and maintain a healthy production environment. Automated PD fault recognition has been carried out through many techniques including Machine Learning (ML) and Deep Learning (DL) as it can be seen in the benchmark Table 1 of many research efforts on PD utilizing Artificial Intelligence (AI) based on Ultrasound data. The contribution of this paper can be summarized into two major points:

1) Validate the capability of CNN structure to detect PD patterns in mixed data collected from the field of different kinds of electrical equipment.
2) Achieve high precision in the detection of PD in the presence of high level of field noise.

The present paper is organized as follows: section II is describing the modeling of PD in addition to data collection methodology and processing. Section III elaborate the proposed approach to detect the PD and the results. Finally, section IV concludes the research work.

II. SYSTEM MODELING

A. PARTIAL DISCHARGE DATA ACQUISITION

Electrical methods for detecting partial discharge are not always effective due to electromagnetic interference, which can be difficult to control in practical field application. Discrimination based on time and frequency domain characteristics is often necessary, and specialized PD couplers may need to be designed to suit the machine. Acoustic PD detection is preferable in many situations because it is immune to electromagnetic interference, does not require large modification for different equipment, can be performed with equipment on the service and can often provide location information for PD sources in complex systems.

Acoustic Emission (AE) discharge detection involves the detection of mechanical wave produced by a discharge event that travels through the insulation to the surrounding vicinity. When sound travels through a medium, it creates a disturbance that propagates through the insulation. This disturbance causes local changes in pressure(P) and density (p), which in turn cause molecules to move and create a wave motion. In liquids, the disturbance leads to compression and refraction of the medium and can be described by general differential equation of acoustic wave motion [26]

$$\nabla^2 p = \frac{1}{c^2}\frac{\partial^2 p}{\partial t^2} \tag{1}$$

where $\nabla^2 p = (\frac{\partial^2 p}{\partial x^2} + \frac{\partial^2 p}{\partial y^2} + \frac{\partial^2 p}{\partial z^2})$, c represents the velocity of the acoustic wave.

there are several graphical modeling of PD, one of the well known models is the Whitehead's three capacitance circuit model [27]. In order to represent the void within an insulation material, a circuit model with 3 capacitances is used. In this model, C1 and C3 are used to describe the capacitance of the healthy insulation and runs in parallel to C4 and C5. On the other hand, C4 and C5 are demonstrating the capacitance of the insulator that is in series with the void C2. This circuit model is illustrated in Fig. 3.

The model can be simplified by using three capacitance equivalent circuit as demonstrated in Fig. 4. C1 and C3 are the capacitance of the healthy insulation that are connected in parallel with C2,C4 and C5 which is represented by C1 in Fig. 4. On the other hand, C4 and C5 represent the insulator capacitance that is connected in series with the void C2, and replaced with C3 in the simplified model.

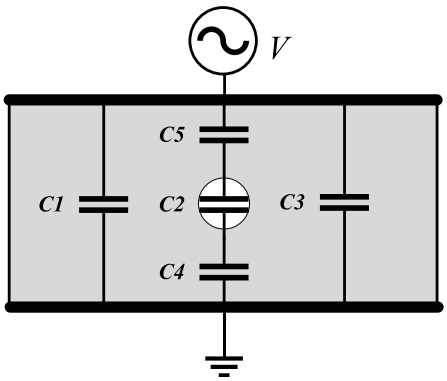

FIGURE 3. PD model.

Before PD event, the voltage across the void is equal to

$$V_v = \frac{X_{C3}}{X_{C2} + X_{C3}} V \tag{2}$$

When PD start developing, the electric field force exerted on the void from the outside suddenly disappears, causing

TABLE 1. Recent researches on PD detection based on acoustic emission and ultrasound.

Ref	Equipment	AI method	Accuracy
[7]	Outdoor Insulator	ANN-BP	85%
[14]	oil-filled submarine cable terminal	ANN-BP	96%
[15]	Power Transformer	KNN/SVM	98%
[16]	High Voltage Bushing	KNN/ANN/SVM & others	95%
[17]	Power Transformer	PCA/KNN	94%
[18]	Power Transformer	GB/RF/SVM& others	>90%
[19]	Power Transformer	IFA	high
[20]	XLPE Cable	CNN	96%
[21]	Transformer Insulation	CNN	88%
[22]	Power Transformer	CNN/DNN/RNN	89-93%
[23]	PD simulator	CNN	74-86%
[24]	Oil Paper Insulation	KNN/MLP& others	92-99%
[25]	Insulation for Transformers	ANN	95%

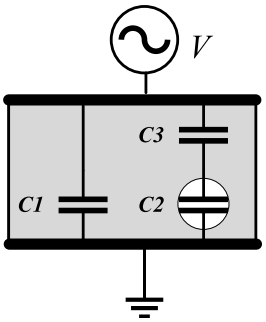

FIGURE 4. PD simplified model.

the void to lose its equilibrium. As a result, the void starts to vibrate due to the elastic force acting on it. This phenomena can be expressed using the following equation:

$$L_m C_m \frac{d^2 u_c}{dt^2} + R_m C_m \frac{du_c}{dt} + u_c = 0 \tag{3}$$

where L_m is the inductance of the mechanical equivelent circuit; C_m represents the elasticity of the system; R_m represents the friction losses; and u_c is the external force on the void wall.

The PD ultrasonic wave is affected by two primary factors, the first factor is the electric field force that happened during the discharge process and the second factor is the pressure wave that results from the expansion of the void or bubble due to the heat of the discharge arc [28].

There are two main types of Ultrasound detection methodology, one is known as structure borne where it detects the propagated waves within the material or through its surface by being attached to the device. This type shows high accuracy in location where direct exposure of the PD is challenging, for instance the switchgears that is on service and difficult to be taken out for inspection. If the PD location is accessible or far away from the sensor, then airborne type is suitable for such applications. Both sensors convert the detected waves into electrical signals, typically using piezoelectric ceramics. This conversion process allows the signals to be analyzed using conventional data acquisition systems. Piezoelectric is a group of materials that exhibit a reversible relationship between mechanical stress and electric force. This behavior is illustrated in Fig. 5, where a cylindrical piezoelectric element with electrodes on both ends is shown. When a voltage is applied to the element through the electrodes, it either expands or contracts in response to the voltage. Conversely, when the shape of the piezoelectric element is deformed by an external force, it generates a voltage. Hence, the piezoelectric element can convert mechanical energy into electrical energy and vice versa which is referred to as the piezoelectric effect. Materials that exhibit this property are called piezoelectric materials. Piezoelectric ceramics are one such type of piezoelectric material [29].

(a) (b)

FIGURE 5. Piezoelectric ceramics basic behavior.

During the AE event, the AE wave generated within a solid material travels through different materials until it reaches the AE sensor made of piezoelectric ceramic. The AE wave deforms the piezoelectric ceramic, producing a voltage signal known as the AE signal. This signal is transmitted through a cable and preamplifier, then the filter remove external signals. After that, it amplifies the signal again to be detected by a measuring instrument as shown in Fig. 6.

The modern PD acoustic detectors are based on a concept called Superheterodyne. Fig.7 shows a circuit of a similar detector that is used to collect the data used in this research. The signal is detected through the transducer then it is amplified before the mixer. In the mixer, multiplying the original signal with local oscillator frequency will generate new two signals with a frequencies that are equal to the summation of the original frequencies and the difference of the two original frequencies. The resultant signal with a lower frequency is audible and will be passed through the filter, the other signal with higher frequency is filtered out. The

resultant signal is amplified later for the final stage before producing the sound for the user [30].

B. PD SIGNAL PREPROCESSING

AE signal waveforms can exhibit a wide range of variations, but they can usually be categorized into specific patterns based on their visual appearance. Although all signals can be categorized as PD, each equipment failing due to PD can produce slightly different waveform. Also, some forms of PD appear on some equipment but not in all, such as tracking can not be seen in transformers internal winding.

All collected samples have been classified into 5 classes; four represents the state of the failure and one represent the healthy state of the equipment. The four classes that represent the failure type are shown in Fig. 8. Time domain waveform is usually investigated to identify the type of failure, but in some cases we refer to frequency waveform to farther assist the waveform because corona in some cases looks similar to tracking but if frequency domain in corona is inspected it can be noticed that the system frequency multiples usually have higher components than other frequencies. The noise level existed is considerable and it might affect the recognition of fault, however adding the step of removing the noise each time we need to classify the fault is not significant for the final accuracy so it is not considered in this work.

The collected samples are diverse which cover a wide range of electrical equipment such as power transformers, switchgears, controlgears, motors, and cables. The collected samples have been processed and classified manually based on general patterns that are usually recognized during the inspection. The frequency response of any waveform is produced by taking the Discrete Fourier transform of time domain waveform as in equation 4 [31], then the negative spectrum of the signal is removed by taking the absolute value of the signal.

$$Y(k) = \sum_{j=1}^{n} X(j) W_n^{(j-1)(k-1)} \tag{4}$$

where $W_n = \exp(-2\pi i)/n$

Arcing waveform is usually recognized as an off and on burst of waves, that is due to the fact that the loose wire or cable starts to build the voltage until the breakdown and then it is emitting a high frequency sound wave as can be seen in Fig. 9. The frequency domain shows clear components at system frequency and around three times the system frequency, however this pattern is not necessary to been seen in all arcing waveforms.

During the event of equipment looseness, the time domain waveform tend to form small triangles of wave burst and the frequency waveform usually has frequency components more than arcing waveform which is again not necessary a multiple of system frequency as depicted in Fig. 10.

In case of corona, the time domain waveform produce peaks on system frequencies which clearly can be observed by investigating the frequency spectrum. Corona produce frequency components on the system frequency and system frequency multiples as it can be seen in Fig. 11. In contrast, tracking waveform is very random and produce high sound intensity with random frequency components which clearly can be seen in Fig. 12.

After processing the signal, the data need to be prepared for Convolution Neural Network (CNN) by converting the waveform into pictures. This step is very important since CNN accept input pictures only, hence three features is extracted from the signals and then converted into pictures. First of all, Short-Time Fourier Transform (STFT) is implemented to preserve the time information. STFT is simply breaking the audio signal into small segments [32] and taking FFT of each segment as per the illustration in Fig. 14 [33].

After Completing the STFT, we start constructing the signal into spectogram where the signal is converted into a usable picture for CNN.

C. CNN ARCHITECTURE AND TUNING

CNN is a deep learning model that is inspired by the visual system of living organisms. This type of neural network has multiple layers and is commonly used in computer vision and natural language processing. Its ability to automatically learn and extract features from images and texts has made it a popular choice for various fields. CNNs use convolutional layers that apply filters to input data to extract meaningful information. The extracted features are then fed into fully connected layers that classify or predict the output. CNNs have been successfully applied to various tasks such as image classification, object detection, and natural language processing [34].

CNN comprises several layers that function as building blocks. More elaboration on some of these building blocks is discussed and their respective roles in the CNN architecture are as follows:

1) CONVOLUTIONAL LAYER

Mathematically, the convolution $(x * w)(a)$ of functions x and w is defined in all dimensions as

$$(x * w)(a) = \int x(t) w(a - t) da \tag{5}$$

The convolutional layer is a crucial element in CNN architecture that plays a vital role in generating an output feature map by convolving a set of convolutional kernels or filters with the input image [35].

2) POOLING LAYER

Pooling layers are an essential component of CNN architectures, which enable sub-sampling of the feature maps obtained after convolution operations. They reduce the size of the feature maps by extracting dominant features in each pool step while maintaining the most important information [36].

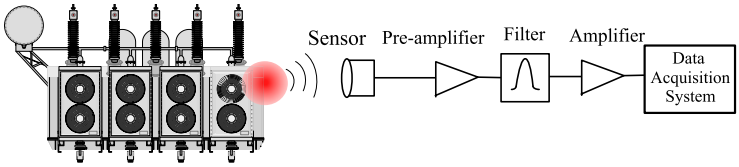

FIGURE 6. working principle of the detection system.

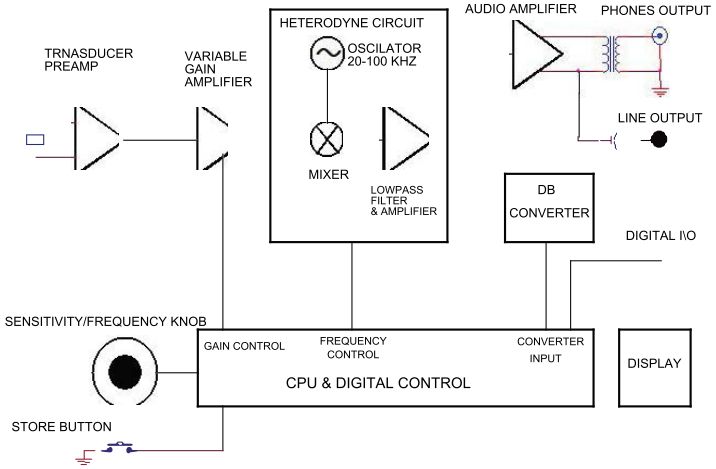

FIGURE 7. Modern PD detector circuit.

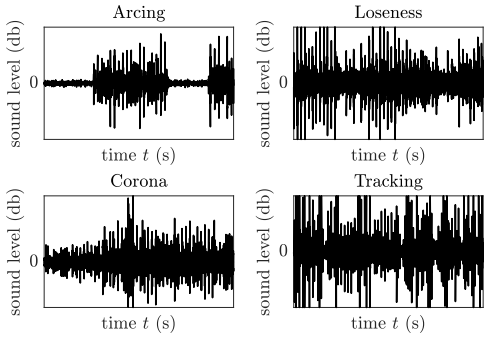

FIGURE 8. Time series waveform of random samples.

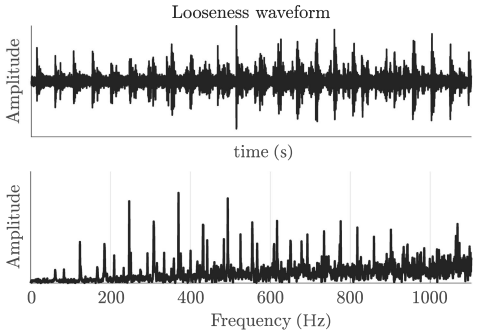

FIGURE 10. Looseness common pattern.

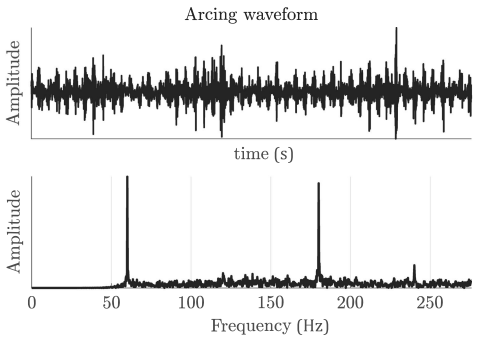

FIGURE 9. Arcing common pattern.

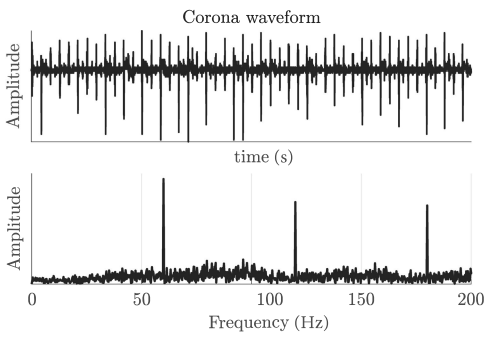

FIGURE 11. Corona common pattern.

3) ACTIVATION FUNCTION

In a neural network, the activation function plays a crucial role in mapping the input to the output. The input is obtained by calculating the weighted sum of the neuron's input, and the bias is added if applicable. The activation function determines whether the neuron will activate or not

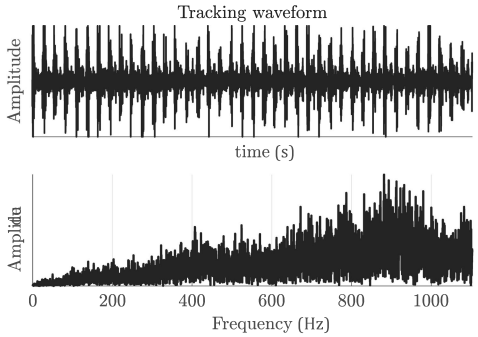

FIGURE 12. Tracking common pattern.

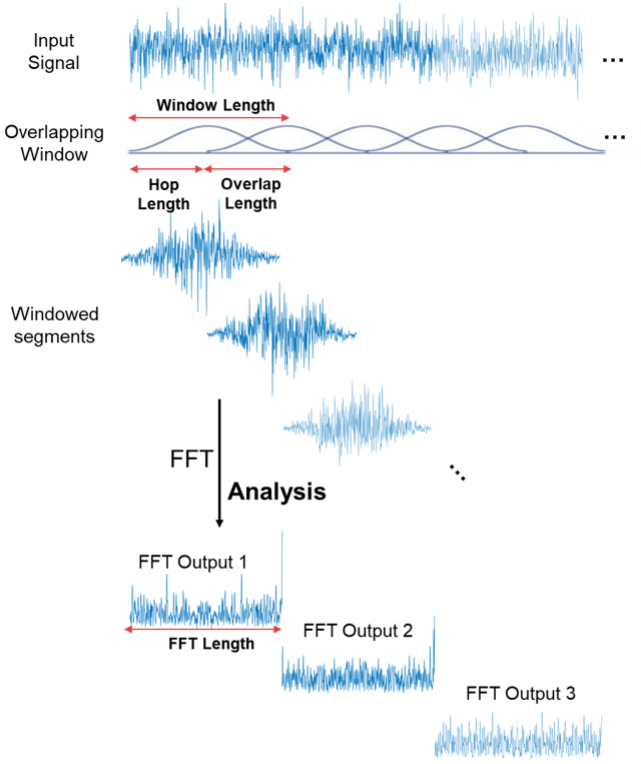

FIGURE 13. STFT concept.

for a given input by generating the corresponding output. Essentially, it transforms the input to the output, allowing for more complex decision-making and non-linearity in the neural network. A Rectifier Linear Unit (ReLU) is a widely used activation function in CNNs. It is designed to convert all negative input values to zero while maintaining positive values. This function is computationally inexpensive compared to other activation functions. Mathematically, ReLU is represented as:

$$f(x)_{ReLU} = max(0, x) \tag{6}$$

4) FULLY CONNECTED LAYER

Typically, the final layers of a CNN architecture used for classification consist of fully-connected layers. Each neuron in a fully-connected layer is connected to every neuron in the previous layer. The last fully-connected layer serves as the output layer, which produces the classification result of the CNN architecture [37]. Fully connected layers can be modeled using the below general equations:

$$\omega_{ij}^{h}(t+1) = \omega_{ij}^{h}(t) + \eta\, x_j\, \varphi' \sum_{k}^{L} (e_k \omega_k i) \tag{7}$$

$$b_{ij}^{h}(t+1) = b_{ij}^{h}(t) + \eta\varphi' \sum_{k}^{L} (e_k \omega_k i) \tag{8}$$

The above equation is used to update wights ω_{ij} and biases b_{ij} which is derived from the least mean square method

$$I = 1/2 \sum_{k}^{L} (Y_k - Y_k^h)^2 \tag{9}$$

there are great number of hyperparameters that can be tuned within CNN architecture. e.g. filter size, number of convolution layers, learning rate, input picture size and number of fully connected neurons. Tuning of these parameters can be done with trail and error, however there are more robust methods that improve the architecture accuracy and reduce the loss in more efficient way such as Bayesian optimization method [38].

Bayesian optimization is an algorithm used to solve global optimization problems by leveraging Bayes Theorem. Global optimization is a complex task that involves finding the input parameters that can minimize or maximize a given objective cost function. Typically, the objective function is characterized by non-convexity, nonlinearity, high-dimensionality, noise, and high computational cost, making it difficult to analyze. Bayesian optimization is an effective approach to address these challenges, as it is able to efficiently and effectively explore the parameter space to identify the optimal set of parameters that can yield the best results [39], [40].

III. PROPOSED APPROACH AND RESULTS

A. SINGLE-PHASE CNN FOR FAULT CLASSIFICATION

The main objective of the model is to classify any detected fault during the equipment operation so the maintenance crew can take action to rectify the issue. Sometimes, the rectification is limited to cleaning the equipment, but other times the rectification involve shutting down the whole process and taking the equipment out of service for extended periods. The ultrasound data is collected from different equipment at different locations and times which reflect the diversity of the data collected as it can be seen in Table 2 and Table 3.

TABLE 2. Number of collected samples for healthy and faulty equipment.

Equipment Condition	Collected Samples
Faulty Equipment	1824
Healthy Equipment	1732

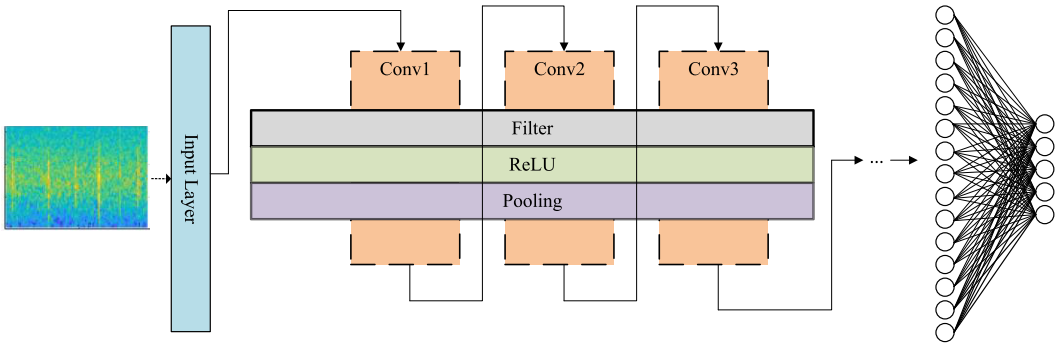

FIGURE 14. CNN general structure.

TABLE 3. Number of collected samples for each type of PD.

PD Type	Collected Samples
Arcing	356
Corona	442
Looseness	506
Tracking	520

The architecture of the network and the main parameters are shown below in Table 4 and Fig. 15:

TABLE 4. Selected parameters for CNN.

Parameter	Selected Value
Number of layers	22
Input layer size	$86 \times 86 \times 3$
1^{st} Convolution Layer size	$86 \times 86 \times 32$
2^{nd} Convolution Layer size	$43 \times 43 \times 64$
3^{rd} Convolution Layer size	$21 \times 21 \times 128$
4^{th} Convolution Layer size	$21 \times 21 \times 128$
1^{st} pooling Layer size	$43 \times 43 \times 32$
2^{nd} pooling Layer size	$21 \times 21 \times 64$
3^{rd} pooling Layer size	$10 \times 10 \times 128$
Fully connected layers/ (neurons in each layer)	$2/(512) - (5)$
Max Epochs	20
Mini-Batch size	32
Training-Validation-Testing percentages	70% - 15% -15%
Validation frequency	10
Initial learning rate	0.001
Learning rate drop factor	0.1
learning rate drop period	15

The selection of CNN parameters for this proposed method is based on trail and error in addition to experts best practices. The four convolution layers in this proposed model can learn several features that are extracted from the acoustic signals e.g. timbral and pitch information that is usually extracted from MFCC and FTT. Fig. 16 shows learned features after each convolution layer, each convolution layer will capture certain picture features like edges and colors. First picture in Fig.16(a), clearly shows the learnable features as mostly colors while as the layers go deeper the learned features turned to be more detailed and complex such as textures and edges in Fig.16(c) and (d).

The training and validation plot showed good improvement of the accuracy and loss function as the number of iterations increase as it can be seen in Fig.18. Table 5 shows the results of CNN model training, validation and final accuracy as well as simulation time:

TABLE 5. Output parameters for single-phase CNN.

Output parameter	Result
Training Accuracy	98%
Validation Accuracy	92%
Training loss	0.038
Validation loss	0.23
Number of iterations	1540
Training time	159 sec

The detection of Tracking failure scored the lowest accuracy due to the randomness of signal detected by ultrasound device, while detecting healthy equipment scored the highest accuracy since the produced signal is unique in terms of the wave form and usually don't produce high frequency signals as it can be seen in Fig 17.

B. DOUBLE-PHASES CNN FOR FAULT CLASSIFICATION

The maintenance crew during the inspection demand the knowledge of one answer as a starting point; is the equipment healthy? in that case, the model can be modified to answer this question in the beginning, then the model as a second phase can identify the type of the fault. This method allow the model to improve the overall accuracy to a very great percentage.

The parameters in Single-Phase model is used as they are except of the output classifier since it is changed to two classifications. The output of the model outperforms the previous single-phase model as it can be seen in Table 6 and Fig. 19. The training and validation plot showed a robust convergence after few iterations, which clearly improve the detection of PD in the equipment.

All PD failures produce high frequency components that easily can be distinguished from the health "silent" waveforms which clearly indicated in the confusion matrix in Fig.20.

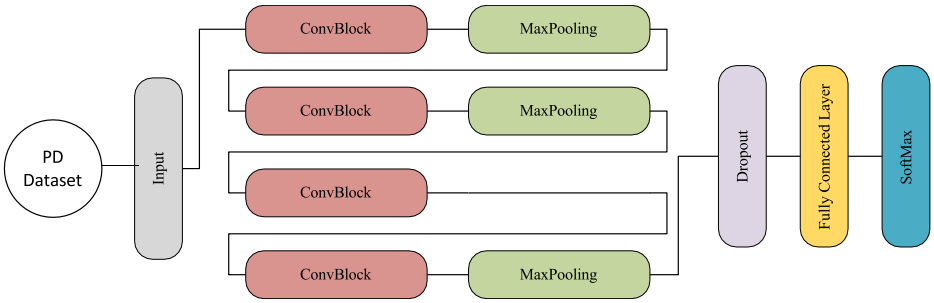

FIGURE 15. CNN architecture for single-phase.

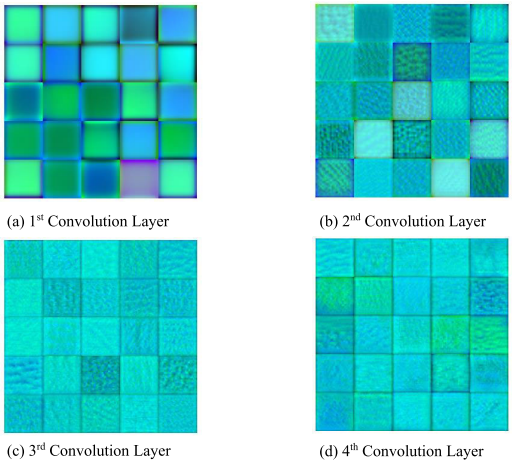

FIGURE 16. Features detection from 1^{st} convolution layer to 4^{th}.

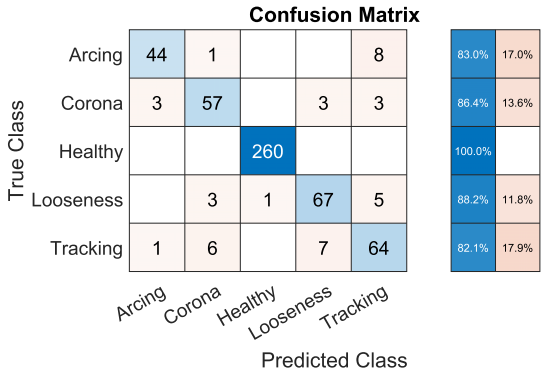

FIGURE 17. Confusion matrix for single-phase validation accuracy.

TABLE 6. Output parameters for double-phase CNN.

Output parameter	Result
Training Accuracy	100%
Validation Accuracy	99.62%
Training loss	9.6×10^{-5}
Validation loss	0.016
Number of iterations	1540
Training time	206 sec

C. ENHANCED SINGLE-PHASE CNN USING BAYESIAN OPTIMIZATION

The goal of the Bayesian optimization technique employed in this research is to minimize the validation classification error, which is set as the objective function. In general, Multiple hyperparameters are decided to be tuned within the selected range in order to achieve the objective function. Four hyperparameters are selected in this model to be optimized, *section depth* decide the depth of the model in terms of number of convolution layers in each section. *Initial learning rate* in the other side will select the hyperparameters are listed in the below Table 7. After optimizing the network, Table 8 shows the outcomes of the optimizer with optimal parameters.

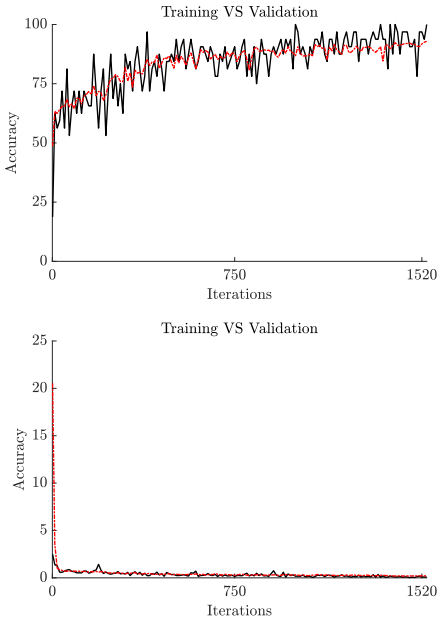

FIGURE 18. Training verses validation accuracy and loss functions.

TABLE 7. Hyperparameters tuning for CNN.

Hyperparameter	Search range	Scale
Section depth	[1 4]	Integer
Initial learning rate	$[1 \times 10^{-3}\ 1]$	Log
Momentum	[0.8 0.98]	Real
Regularization	$[1 \times 10^{-10}\ 1 \times 10^{-2}]$	Log

The optimized hyperparameters produced better model with improved accuracy as well as loss value as per Table 9.

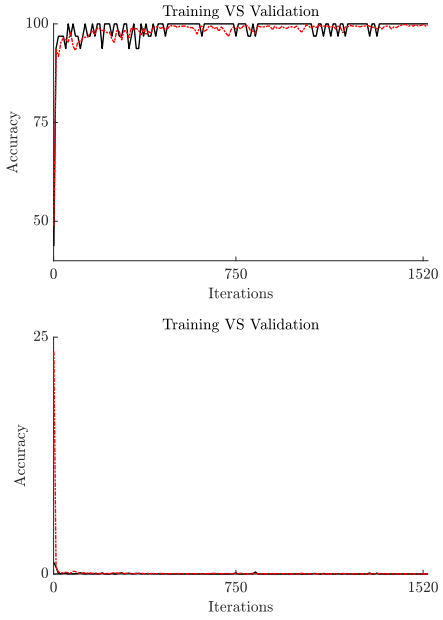

FIGURE 19. Training verses validation accuracy and loss functions.

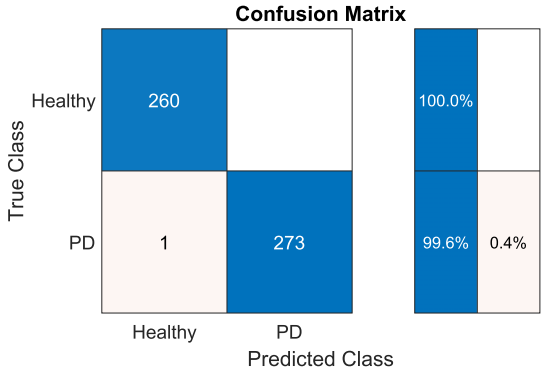

FIGURE 20. Confusion matrix for double-phase validation accuracy.

TABLE 8. Optimal parameters for CNN.

Hyperparameter	Optimal value
Section depth	2
Initial learning rate	0.0042
Momentum	0.8035
Regularization	1.237

The objective function progress through the optimization process is shown in Fig. 21

TABLE 9. Comparison between single-phase and optimized models CNN.

Output parameter	Single-Phase Model	Optimized model
Validation Accuracy	92%	94%
Validation loss	0.23	0.058
Training time	159 sec	4501 sec

The overall accuracy is improve as well as the validation accuracy of each PD type when compared with Single-Phase

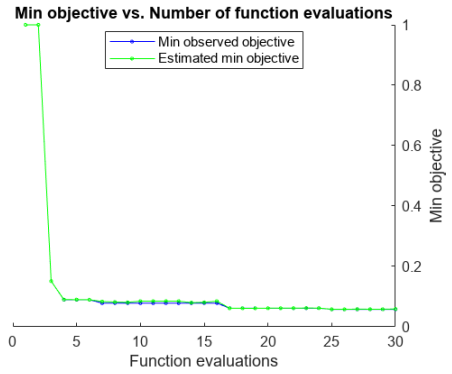

FIGURE 21. Function evaluations throughout the iterations.

case. Tracking detection accuracy is improved by far when compared to other PD types as it can be seen in Fig. 22

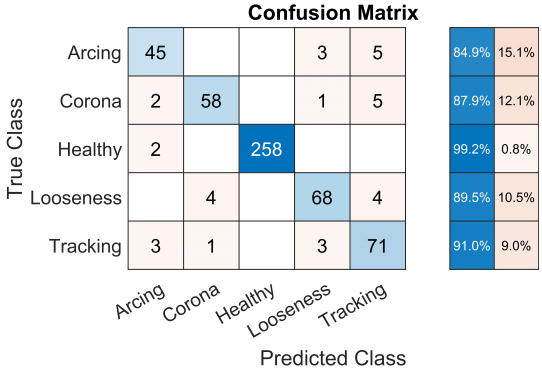

FIGURE 22. Confusion matrix for Optimized double-phase validation accuracy.

D. BENCHMARK WITH PRETRAINED MODELS

There are existing models that have been trained and developed on audio classification for many general applications [41]. In order to investigate the performance of the developed models, the same collected data have been trained and validated with latest state-of-the-art audio classification pretrained models and compared with the developed models as shown in Fig 23. Below is a summary of each model:

- **VGGish** represents a Convolutional Neural Network (CNN) that has been pre-trained by Google. Its architecture takes cues from the well-known VGG networks extensively utilized for image classification tasks. The structure of VGGish encompasses a sequence of convolutional and activation layers, with the possibility of including a subsequent max pooling layer. In its entirety, this neural network consists of a total of 17 layers [42].
- **OpenL3** is a freely available deep audio embedding framework developed as an open-source project. It builds upon the self-supervised L3-Net and introduces enhancements to its architecture. OpenL3 surpasses the performance of VGGish, SoundNet, and even the original L3-Net on various sound recognition tasks [43].
- **YamNet** (Yet Another Mobile Network), abbreviated as YAMNet, is a pre-trained model designed for acoustic

detection. It is trained by Dan Ellis using the AudioSet dataset, which consists of labeled data sourced from over 2 million YouTube videos. YAMNet utilizes the depth-wise-separable convolution architecture of MobileNet_v1. This architecture allows for efficient computation and reduces the number of parameters in the model, making it suitable for mobile and resource-constrained environments [44].

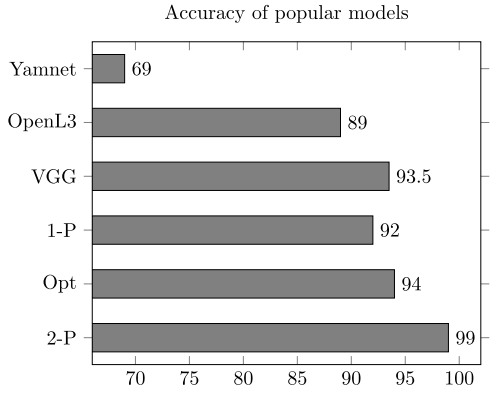

FIGURE 23. Benchmarking the percentage accuracy of proposed models with pretrained models.

IV. CONCLUSION

In this work, four different types of PD have been collected of a diverse number of electrical equipment from the actual field environment where noise is a major challenge. Each type of PD produce a unique audio signal that is possible to be detected by ultrasound detector. In this work, a general observation on the audio signals have been reported in order to be classified before the preprocessing of the data. After the processing stage, a novel methodology have been implemented to preprocess the data using three different features which are STFT, MFCC and PSD. In the final stage, three different proposed approaches have been discussed which are the Single-Phase CNN, Double-Phase CNN and Optimized Single-Phase CNN. The proposed approaches have showed higher accuracy in comparison with a state-of-the-art pretrained models.

ACKNOWLEDGMENT

The authors would like to acknowledge the support provided by the Deanship of Research Oversight and Coordination (DROC) at King Fahd University of Petroleum & Minerals (KFUPM) for funding this work through project No. SL222001. The authors greatly value and acknowledge the data provided and the feedback from Ultrasound experts Eng. Ahmad Moataz and Eng. Ahmad Hassan in addition to UE Systems Inc.

REFERENCES

[1] X. Zhang, B. Pang, Y. Liu, S. Liu, P. Xu, Y. Li, Y. Liu, L. Qi, and Q. Xie, "Review on detection and analysis of partial discharge along power cables," *Energies*, vol. 14, no. 22, p. 7692, Nov. 2021.

[2] B. Fruth, "Partial discharge mechanisms in solid insulation systems," in *Proc. 4th Int. Conf. Conduction Breakdown Solid Dielectr.*, Jun. 1992, pp. 297–307.

[3] *What is Partial Discharge*, Omicron, Vancouver, BC, Canada, Feb. 2020.

[4] V. B. Rathod, G. B. Kumbhar, and B. R. Bhalja, "Partial discharge detection and localization in power transformers based on acoustic emission: Theory, methods, and recent trends," *IETE Tech. Rev.*, vol. 39, no. 3, pp. 540–552, May 2022.

[5] M. Shafiq, G. A. Hussain, L. Kütt, and M. Lehtonen, "Effect of geometrical parameters on high frequency performance of Rogowski coil for partial discharge measurements," *Measurement*, vol. 49, pp. 126–137, Mar. 2014.

[6] B. Qi, C. R. Li, Z. Hao, B. B. Geng, D. G. Xu, S. Y. Liu, and C. Deng, "Surface discharge initiated by immobilized metallic particles attached to gas insulated substation insulators: Process and features," *IEEE Trans. Dielectr. Electr. Insul.*, vol. 18, no. 3, pp. 792–800, Jun. 2011.

[7] S. Polisetty, A. El-Hag, and S. Jayram, "Classification of common discharges in outdoor insulation using acoustic signals and artificial neural network," *High Voltage*, vol. 4, no. 4, pp. 333–338, Dec. 2019.

[8] Z. Liu, Y. Wang, X. Chen, X. Meng, X. Liu, and J. Yao, "An optical fiber sensing method for partial discharge in the HVDC cable system," *Int. J. Electr. Power Energy Syst.*, vol. 128, Jun. 2021, Art. no. 106749.

[9] S. F. Stefenon, R. Z. Freire, L. H. Meyer, M. P. Corso, A. Sartori, A. Nied, A. C. R. Klaar, and K.-C. Yow, "Fault detection in insulators based on ultrasonic signal processing using a hybrid deep learning technique," *IET Sci., Meas. Technol.*, vol. 14, no. 10, pp. 953–961, Dec. 2020.

[10] J. Faiz and M. Soleimani, "Assessment of computational intelligence and conventional dissolved gas analysis methods for transformer fault diagnosis," *IEEE Trans. Dielectr. Electr. Insul.*, vol. 25, no. 5, pp. 1798–1806, Oct. 2018.

[11] J. Cai, L. Zhou, J. Hu, C. Zhang, W. Liao, and L. Guo, "High-accuracy localisation method for PD in transformers," *IET Sci., Meas. Technol.*, vol. 14, no. 1, pp. 104–110, Jan. 2020.

[12] Y. O. Shaker, "Detection of partial discharge acoustic emission in power transformer," *Int. J. Electr. Comput. Eng. (IJECE)*, vol. 9, no. 6, p. 4573, Dec. 2019.

[13] H. Song, J. Dai, G. Sheng, and X. Jiang, "GIS partial discharge pattern recognition via deep convolutional neural network under complex data source," *IEEE Trans. Dielectr. Electr. Insul.*, vol. 25, no. 2, pp. 678–685, Apr. 2018.

[14] Y. Wang, X. Zhang, Y. Li, L. Li, J. Gao, and N. Guo, "Multi-scale analysis and pattern recognition of ultrasonic signals of PD in a liquid/solid composite of an oil-filled terminal," *Energies*, vol. 13, no. 2, p. 366, Jan. 2020.

[15] M. Kunicki and D. Wotzka, "A classification method for select defects in power transformers based on the acoustic signals," *Sensors*, vol. 19, no. 23, p. 5212, Nov. 2019.

[16] R. Hussein, K. B. Shaban, and A. H. El-Hag, "Robust feature extraction and classification of acoustic partial discharge signals corrupted with noise," *IEEE Trans. Instrum. Meas.*, vol. 66, no. 3, pp. 405–413, Mar. 2017.

[17] M. Harbaji, K. Shaban, and A. El-Hag, "Classification of common partial discharge types in oil-paper insulation system using acoustic signals," *IEEE Trans. Dielectr. Electr. Insul.*, vol. 22, no. 3, pp. 1674–1683, Jun. 2015.

[18] W. L. Woon, A. El-Hag, and M. Harbaji, "Machine learning techniques for robust classification of partial discharges in oil–paper insulation systems," *IET Sci., Meas. Technol.*, vol. 10, no. 3, pp. 221–227, May 2016.

[19] Y.-B. Wang, D.-G. Chang, S.-R. Qin, Y.-H. Fan, H.-B. Mu, and G.-J. Zhang, "Separating multi-source partial discharge signals using linear prediction analysis and isolation forest algorithm," *IEEE Trans. Instrum. Meas.*, vol. 69, no. 6, pp. 2734–2742, Jun. 2020.

[20] Q. Che, H. Wen, X. Li, Z. Peng, and K. P. Chen, "Partial discharge recognition based on optical fiber distributed acoustic sensing and a convolutional neural network," *IEEE Access*, vol. 7, pp. 101758–101764, 2019.

[21] W. L. Woon, Z. Aung, and A. H. El-Hag, "Intelligent monitoring of transformer insulation using convolutional neural networks," in *Proc. 6th ECML PKDD Workshop, DARE*, Dublin, Ireland, Sep. 2018, pp. 127–136, doi: 10.1007/978-3-030-04303-2_10.

[22] Q. Zhang, J. Lin, H. Song, and G. Sheng, "Fault identification based on PD ultrasonic signal using RNN, DNN and CNN," in *Proc. Condition Monitor. Diagnosis (CMD)*, Sep. 2018, pp. 1–6.

[23] M. Borghei and M. Ghassemi, "A deep learning approach for discrimination of single- and multi-source corona discharges," *IEEE Trans. Plasma Sci.*, vol. 49, no. 9, pp. 2936–2945, Sep. 2021.
[24] T. Boczar, S. Borucki, D. Jancarczyk, M. Bernas, and P. Kurtasz, "Application of selected machine learning techniques for identification of basic classes of partial discharges occurring in paper-oil insulation measured by acoustic emission technique," *Energies*, vol. 15, no. 14, p. 5013, Jul. 2022.
[25] T. Boczar, S. Borucki, A. Cichon, and D. Zmarzly, "Application possibilities of artificial neural networks for recognizing partial discharges measured by the acoustic emission method," *IEEE Trans. Dielectr. Electr. Insul.*, vol. 16, no. 1, pp. 214–223, Feb. 2009.
[26] L. E. Lundgaard, "Partial discharge. XIII. Acoustic partial discharge detection-fundamental considerations," *IEEE Elect. Insul. Mag.*, vol. 8, no. 4, pp. 25–31, Jul. 1992.
[27] H. N. Afrouzi, A. Hassan, D. T. Y. Chee, K. Mehranzamir, Z. A. Malek, S. V. Mashak, and J. Ahmed, "In-depth exploration of partial discharge modelling methods within insulations," *Cleaner Eng. Technol.*, vol. 6, Feb. 2022, Art. no. 100390.
[28] Y. Wang, X. Li, Y. Gao, H. Zhang, D. Wang, and B. Jin, "Partial discharge ultrasound detection using the Sagnac interferometer system," *Sensors*, vol. 18, no. 5, p. 1425. Apr. 2018. [Online]. Available: https://www.mdpi.com/1424-8220/18/5/1425
[29] H. Inaba, "AE sensor (AE transducer)," in *Practical Acoustic Emission Testing*. Tokyo, Japan: Springer, 2016, pp. 35–43.
[30] C. Stagner, A. Conrad, C. Osterwise, D. G. Beetner, and S. Grant, "A practical superheterodyne-receiver detector using stimulated emissions," *IEEE Trans. Instrum. Meas.*, vol. 60, no. 4, pp. 1461–1468, Apr. 2011.
[31] M. Frigo and S. G. Johnson, "The design and implementation of FFTW3," *Proc. IEEE*, vol. 93, no. 2, pp. 216–231, Feb. 2005.
[32] J. B. Allen and L. R. Rabiner, "A unified approach to short-time Fourier analysis and synthesis," *Proc. IEEE*, vol. 65, no. 11, pp. 1558–1564, 1977.
[33] *Short-Time FFT*. (2019). [Online]. Available: https://www.mathworks.com/help/dsp/ref/dsp.stft.html
[34] J. Gu, Z. Wang, J. Kuen, L. Ma, A. Shahroudy, B. Shuai, T. Liu, X. Wang, L. Wang, G. Wang, J. Cai, and T. Chen, "Recent advances in convolutional neural networks," *Pattern Recognit.*, vol. 77, pp. 354–377, May 2018.
[35] A. Ghosh, A. Sufian, F. Sultana, A. Chakrabarti, and D. De, "Fundamental concepts of convolutional neural network," in *Recent Trends and Advances in Artificial Intelligence and Internet of Things*. Cham, Switzerland: Springer, 2020, pp. 519–567.
[36] J. Teuwen and N. Moriakov, "Convolutional neural networks," in *Handbook of Medical Image Computing and Computer Assisted Intervention*. Amsterdam, The Netherlands: Elsevier, 2020, pp. 481–501.
[37] H. Sinha, V. Awasthi, and P. K. Ajmera, "Audio classification using braided convolutional neural networks," *IET Signal Process.*, vol. 14, no. 7, pp. 448–454, Sep. 2020.
[38] H. Cho, Y. Kim, E. Lee, D. Choi, Y. Lee, and W. Rhee, "Basic enhancement strategies when using Bayesian optimization for hyperparameter tuning of deep neural networks," *IEEE Access*, vol. 8, pp. 52588–52608, 2020.
[39] T. Kim, J. Lee, and Y. Choe, "Bayesian optimization-based global optimal rank selection for compression of convolutional neural networks," *IEEE Access*, vol. 8, pp. 17605–17618, 2020.
[40] W. Jia, C. Xiu-Yun, Z. Hao, X. Li-Dong, L. Hang, and D. Si-Hao, "Hyperparameter optimization for machine learning models based on Bayesian optimization," *J. Electron. Sci. Technol.*, vol. 17, no. 1, pp. 26–40, 2019.
[41] E. Tsalera, A. Papadakis, and M. Samarakou, "Comparison of pre-trained CNNs for audio classification using transfer learning," *J. Sensor Actuator Netw.*, vol. 10, no. 4, p. 72, Dec. 2021.
[42] S. Hershey, S. Chaudhuri, D. P. W. Ellis, J. F. Gemmeke, A. Jansen, R. C. Moore, M. Plakal, D. Platt, R. A. Saurous, B. Seybold, M. Slaney, R. J. Weiss, and K. Wilson, "CNN architectures for large-scale audio classification," in *Proc. IEEE Int. Conf. Acoust., Speech Signal Process. (ICASSP)*, Mar. 2017, pp. 131–135.
[43] A. L. Cramer, H.-H. Wu, J. Salamon, and J. P. Bello, "Look, listen, and learn more: Design choices for deep audio embeddings," in *Proc. ICASSP - IEEE Int. Conf. Acoust., Speech Signal Process. (ICASSP)*, May 2019, pp. 3852–3856.
[44] *Sound Classification with YAMNet*. [Online]. Available: https://www.tensorflow.org/hub/tutorials/yamnet

ABDULAZIZ H. ALSHALAWI was born in Taif, Saudi Arabia, in 1992. He received the B.S. degree in applied electrical engineering from the King Fahd University of Petroleum and Minerals (KFUPM), in 2016, where he is currently pursuing the M.S. degree in power systems engineering.

From 2016 to 2023, he was with Saudi Aramco Company, where he was assigned to different roles, including a Technical Specialist Engineer, an Energy Coordinator, a Maintenance Engineer, and an Operations Engineer. He was involved in the development of mega projects and he enhanced the existing system operation and reliability. He was the author and coauthor of several articles and he filed one patent. Since 2023, he has been the Project Manager for renewable projects with Principal Buyer Company to manage the development of utility-scale renewable projects including solar, wind, and energy storage systems. His research interests include AI detection of power systems failures, renewable energy integration, microgrid control, steady state analysis, and power systems optimization. He is the Certified Energy Manager (CEM) of IEA and a licensed PE Engineer at NCEES.

FAHAD S. AL-ISMAIL (Senior Member, IEEE) received the B.Sc. and M.Sc. degrees in electrical engineering from the King Fahd University of Petroleum and Minerals (KFUPM), Saudi Arabia, in 2009 and 2012, respectively, and the Ph.D. degree in electrical engineering from Texas A&M University, College Station, TX, USA, in December 2016. He is currently an Associate Professor and the Director of the Center for Environment and Marine Studies (CEMS), Research Institute (RI), Department of Electrical Engineering, KFUPM. From January 2019 to August 2020, he was the Director of the Energy Research and Innovation Center, KFUPM, which the King Abdullah City for Atomic and Renewable Energy (K. A. CARE) sponsored. He specializes in teaching courses related to energy efficiency, demand-side management, power system operation and control, and power system planning. His research interests include power system planning and reliability, renewable energy integration, energy storage system planning and operation, demand-side management modeling with intermittent resources, and uncertainty representation of renewable energy.